Journal of the Serbian Chemical Society
JSCS-info@shd.org.rs • www.shd.org.rs/JSCS
J. Serb. Chem. Soc. *89* (2) 245–258 (2024)
JSCS–5718
Original scientific paper
Published 2 March 2024

Inhibition study of curcumin extract's effect on dissimilar aluminium joint

KAMATCHI PRAVINKUMAR*, VADDI SESHAGIRI RAO and RENGARAJAN SATHISH

Department of Mechanical Engineering, St. Joseph's College of Engineering, OMR, Chennai-119, India

(Received 24 April, revised 1 June, accepted 8 October 2023)

Abstract: Aluminium welded joints are offering greater interest to researchers owing to the replacement of heavy steel structures and reduction in the weight of the components used in the automobile and marine environments. In this study AA6061 and AA8011 have been welded by using the bobbin tool friction stir welding method and by varying the process parameters with the samples being subjected to corrosion environments. The corrosive nature of the welded alloys in the absence and presence of inhibitors (curcumin) has been examined by electrochemical methods and compared with raw samples. The ratio has been observed between 0.075 and 5.42 A cm^{-2}. The results reveal that corrosion control tendency has been improved by the AA6061 and AA8011 aluminium alloy joint in the presence of curcumin extract.

Keywords: Bobbin tool; aluminium alloys; Tafel plot; scanning electron microscopy.

INTRODUCTION

Researchers are facing many issues between economic growth and natural resource conservation while designing materials for constructive applications. In the 20th century, the climate change was considered to be a serious problem due to industrialization and globalization. Several studies were undertaken to improve the system's performance and the lifetime of the equipment. The efficiency or lifetime can be increased by altering the source metals by adding the minimum weight of low-density components such as aluminium, magnesium alloys and thin-walled components. Apart from various metals, aluminium alloys are used in the aeronautical field such as the construction of rocket fuel tanks owing to their superior strength, extraordinary fracture toughness, and stress corrosion cracking and durability.[1] Though aluminium alloys are exhibiting significant, desirable

* Corresponding author. E-mail: pravinkumark@stjosephs.ac.in
https://doi.org/10.2298/JSC230424074P

properties, they are not without limitations such as surface degradation under working conditions, lower durability at high temperatures and lower wear resistance.[2] The modifications of the Al alloys are receiving good attention of the researchers for mechanical applications.[3] Aluminium alloys (ALA) such as 2XXX series (copper-based), 6XXX series, heat treatable and weldable and 8XXX series (iron-based), are used in most of the mechanical designs in manufacturing industries.[4] This component's structure lets modern technologies link comparable or dissimilar materials using solid-state joining methods, which are better than fusion welding.[5] Recently, various processes such as friction stir welding (FSW), friction surfacing, linear friction welding, and rotary friction welding have been used for joining or coating the surface.[6] Due to its solid-state nature, friction stir welding may combine magnesium and aluminium alloys without flaws.[7] FSW of aluminium alloys has been extensively studied for microstructure evolution and mechanical characteristics.[8] Though it possesses the quality of the joint, there are a few limitations such as the need for a backing plate that influences the flow of grain in the nugget zone, multi passes required to join thick plates, the occurrence of root flaws, and weaker heat generation due to a single shoulder. Bobbin tool friction stir welding (BOBTFSW) is a unique take on the commonplace method of friction stir welding. BOBTFSW has many advantages to conventional friction stir welding (CFSW).[9] Bobbin tool friction stir welding (BOBTFSW) is FSW with different tool morphology.[10] The BOBTFSW tool has two shoulders (upper and lower) and a probe, while the FSW standard tool has a shoulder and a probe. These shoulders touch the work piece's top and bottom. The lower shoulder replaces the FSW backing anvil. BOBTFSW's unique force system makes it more sophisticated than FSW.

Generally, aluminium alloys are resistant to corrosion due to the high reactiveness of oxygen and form a thin layer of oxides, but the material is subjected to service temperature which deteriorates its tensile strength and corrosion resistance property. The novelty of this work is to analyse the behaviour of weld joints which are made by a specially designed bobbin tool on AA6061-T6 and AA8011-H14 aluminium alloys in 1M sodium chloride solution at 25 °C. As stated in the earlier reports, only the electrochemical study was used on samples to explain the potentiodynamic polarization curve.[11] Curcumin with zinc sulphate as an inhibitor on dissimilar aluminium weld joints has not been documented in the literature. The welded sample's Tafel graphs are plotted using potentiodynamic data and the parameters will be compared between the raw sample in salt water and the sample with inhibition with salt water.

EXPERIMENTAL

Materials and methods

The dissimilar grade of aluminium alloys of AA6061-T6 and AA8011-H14 grade was ordered and received in the form of plates with a size of 300 mm×300 mm×5 mm thickness.

AA6061 Aluminium forms a quasi-binary combination $AlMg_2Si$ with "balanced" Mg and Si.[12] Aluminium AA8011 is a high-grade alloy that can be used for bobbin tool welding. It was used to prepare the corrosion resistance test specimens from matrix material with iron and silicon alloying elements (Al6 (Fe,Mn)).[13]

The surface to be welded was polished and cleaned with silicon carbide paper and acetone. The BOBTFSW welding process set-up is shown in Fig. 1a. The tool's upper and lower shoulders have a diameter of 24 mm and a thickness of 5 mm. The pin having a diameter of 9 mm and a length of 5mm shown in Fig. 1b and a hardened cylindrical tool shown in Fig. 1c with a hardness of 59 HRC was selected. The alloys, AA6061 and AA8011 specimen plates were wire cut to a precise size of 100 mm×50 mm×5 mm is shown in Fig. 1d. The welding speed at the start was low and it grew to the desired speed. After welding, the metallographic samples were cut perpendicularly, polished and etched with Keller's reagent (2 ml HF, 3 ml HCl, 5 ml HNO_3, 190 ml H_2O) for 13 s. The welded specimens were subjected to the potentiodynamic polarization study. BOBTFSW welded test specimens with an area of 1 cm^2 were used as the working electrode.[14]

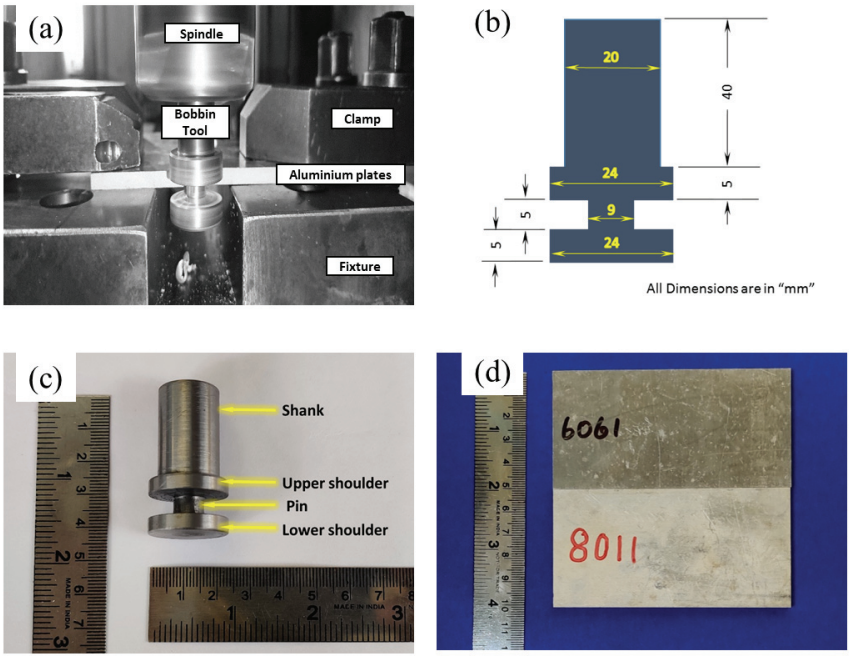

Fig. 1. a) BOBTFSW process; b) nomenclature of BOBTFSW; c) Bobbin tool; d) materials used for welding.

Bobbin tool welding and test specimen preparation

Fig. 2a illustrates the overview of the BOBTFS welding process using AA6061 and AA8011 alloys. The BOBTFSW alloys were nicely welded on both sides, with minor overlaps on the retreating side (RS) and a smooth interface on the advancing side (AS). Consistent arc patterns were observed on both sides, and the distance between arcs rose with a constant traverse speed of 40 mm min^{-1}. The samples were welded by varying the rotational speed from

600 to 1050 rpm. The surface of the tool increased plasticized metal to flow around the stirring pin, which reduced metal fill at the joint nearby area.[23] Because the greater welding rate provided less frictional heat, the specimen welded at a constant 40 mm/min had narrower heat-affected zone widths on both the AS and RS. Hence, this research selected seven samples out of ten for the corrosion-related potentiodynamic study.

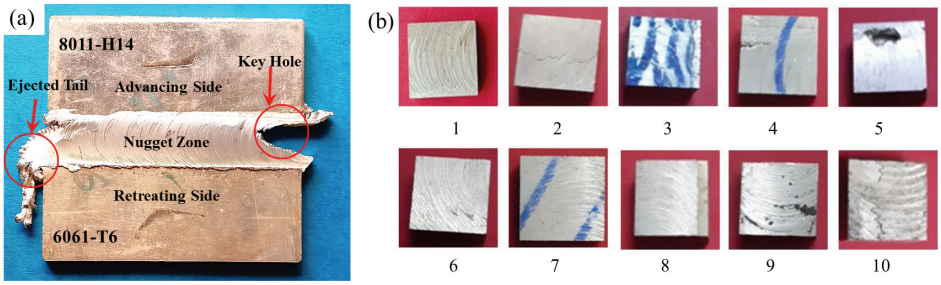

Fig. 2. a) Various zones in BOBTFS welded AA6061 and AA8011 aluminium alloys specimen; b) BOBTFS welded test specimens at various rpm and constant traverse speeds.

After the welding, the samples were sized as 1 cm×1 cm×0.5 cm as dimensions shown in Fig. 2b and subjected to the corrosion investigations. From the ten welded samples, S2, S3, S5, S6, S7, S9 and S10 were selected in the increasing order of their speed of rotation at constant traverse speeds for the corrosion investigation to find the effective rotational speed shown in Table I. The samples' potentiodynamic study in the presence and absence of inhibitors was carried out for stable mechanical design. In order to observe the welded samples' surface morphology, three different rotational speeds of 600, 850 and 1050 rpm of test specimens were used in Quanta 200 FEG-SEM.

TABLE I. Various BOBTFSW samples at constant traverse speed of 40 mm min^{-1} and different rpm

Ser. no.	rpm
1	600
2	650
3	700
4	750
5	800
6	850
7	900
8	950
9	1000
10	1050

Preparation of zinc sulphate solution and inhibitor solution

1.1 g of $ZnSO_4 \cdot 7H_2O$ was dissolved in 250 ml of distilled water and diluted for the corrosion inhibition investigation. 5 ml of this solution diluted to 100 ml gives 50 ppm of Zn^{2+}. 50 g of turmeric powder was boiled with distilled water and the suspending particles

were removed by filtration. The filtrate was used as an inhibitor solution and carried out for a potentiodynamic polarization study with the welded samples. The major chemical component of turmeric is curcumin and its tautomerism is shown in Fig. 3.

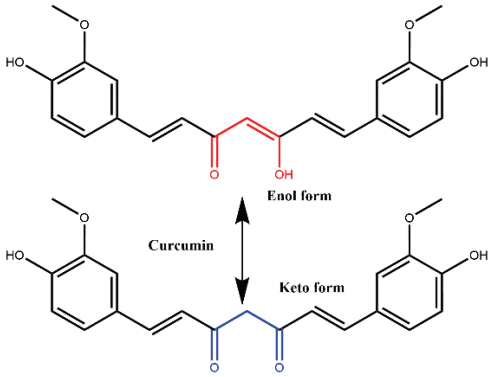

Fig. 3. Structure and keto-enol tautomerism of curcumin.

Potentiodynamic polarization and Tafel study

Electrochemical impedance spectroscopy (EIS) testing employed CH instruments electrochemical workstation system. The working area and metal specimens were immersed in 1 M saltwater electrolyte for 30 min and 1 h, respectively, before measurement. EIS studies at a constant potential used 10 mV excitation signals from 1 kHz to 100 MHz. Based on the charge transfer resistance, the impedance measurements were used to calculate the inhibition percentage. Welded samples were made using commercially pure rods and welded. The specimen for corrosion was prepared for 1 cm^2 active surfaces. Welded samples were impregnated with epoxy resin for electrochemical analysis. Then they were ground on water-resistant SiC abrasive paper to achieve an adequate surface finish. After grinding, the samples were rinsed, degreased and dried. Electrochemical tests were conducted in 1 M sodium chloride solution and the potentials are referred to saturated calomel reference electrode. Analytical purity reagents with 15 μS cm^{-1} demineralized water were used as electrolytes. A similar study was conducted in the presence of a curcumin and zinc salt mixture.[16] The obtained Tafel graphs were interpreted for the corrosion protective sample identification.

To determine the microcell corrosion rates, the reported polarization technique was conducted using the welded test specimens.[17,18] At room temperature, mirror-finished surfaces of BOBTF cuboid specimens and base metals were permitted to come into contact with varied quantities of selected 1 M sodium chloride electrolyte. In order to obtain a stable open circuit potential (OCP), the specimens were exposed to their respective electrolyte solutions for a period of 400 s. For the purpose of recording polarization curves, the specimens were polarized to a potential of 250 mV cathodically and 250 mV anodically with respect to OCP at a scan rate of 1 mV s^{-1}.

RESULTS AND DISCUSSION

This work has successfully welded the two dissimilar aluminium metals AA6061 and AA8011 for mechanical applications. By using this BOBTFS technique, this work has prepared the samples with symmetric thickness and low

distortion without the high force for fastening the selected aluminium plates. It is possible to make efficient use of the heat that is created since the backing plate does not cause any convection loss. Through this welding, the presence of dual rotational shoulders makes the specimens possible to weld alloys with a high melting temperature.[19,20]

The surface morphology of BOBTFS welded samples like low (600 rpm), medium (850 rpm) and higher (1050 rpm) was analysed using SEM.[21] Field emission scanning electron microscope (FESEM) images of selected welded samples are given in Figs. 4a–c. The SEM images have exposed fracture surfaces in different grain sizes due to the heat variation with respect to the rotation of 600 rpm. In Fig. 4a the sample exhibits that dynamic recrystallization in the stir zone area is low and grain size is big owing to minimum heat input. The weak area between the stir zone and mechanically affected zone fractures because the tool's relative displacement is highest in each spinning circle and its extrusion force on the metal conveyed by stirring decreases. Fig. 4b and c have demonstrated that the ductile fracture has several small, shallow dimples with the layered distribution. Likewise, 800 rpm and the highest 1050 rpm have shown dynamic recrystallization which formed fine grains that strengthen the welded zone. Heat input dissolves the stronger phase, increasing the heat-affected zone particle size.[22,23]

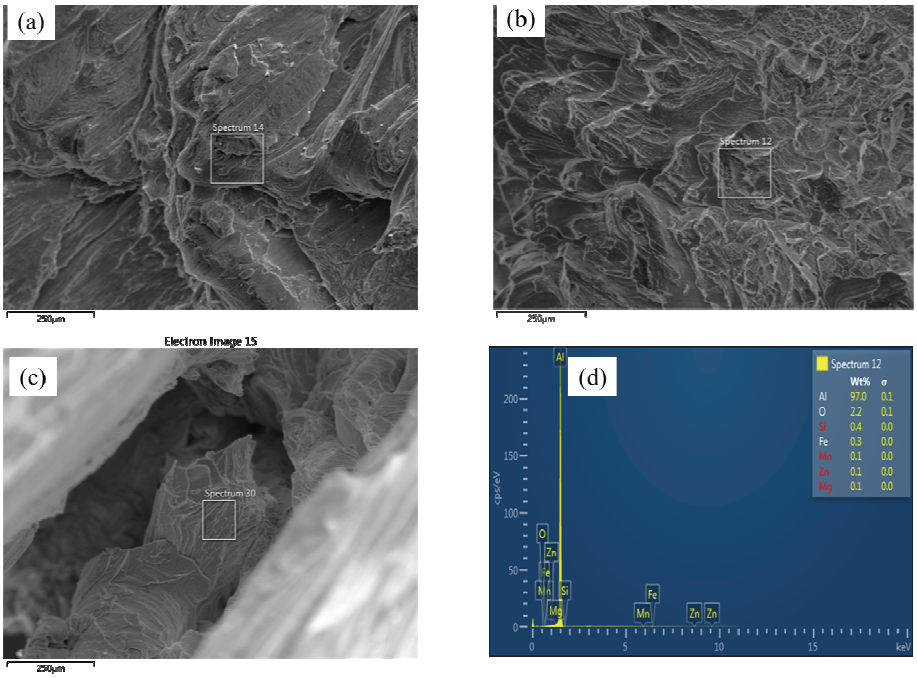

Fig. 4. Surface morphology of 250μm expanded SEM images of: a) 600, b) 850 and c) 1050 rpm welded samples; d) EDX of 850 rpm welded sample.

The samples revealed full penetration through the joint line, which gets rid of root difficulties as well as kissing bond mistakes, both of which are often seen in BOBTFW joints. Moreover, full penetration through the joint line removes any gaps between the joints. It is possible to readily weld thick parts due to the enhanced and balanced heat input at either side (both sides of the plate). This eliminates the need for numerous passes, which enables the complete weld penetration to be achieved in a single pass. In addition to this, the corrosion study was conducted to measure the sample life in NaCl solution and an electrochemical measuring instrument was used for the welded samples to optimize. The measurements of electrochemical polarization yielded corrosion potentials and current data which are used to construct the Tafel plot. According to the reported methods and results, the Tafel outcomes were interpreted.[24,25] The plotting was done for potential *vs.* log *I* values for the prepared welded samples in 1 M sodium chloride solution along with base metals such as AA8011 and AA6061. The graph potential exists (*x*-axis) between –1.5 and –0.5 V. Similarly, the log of current is observed between –1 and –10 A cm^{-2}. From the plotted graph, this work observed the potential of E_{cor} = –1.12 V and E_{cor} = –1.14 V for base metals such as AA8011 and AA6011. Similarly, the welded samples have exposed the same anodic (right) curve and different in the cathodic curve (left). In the absence of an inhibitor, the seven test specimens have shown a corrosion potential between –0.949 (sample 2) and –1.071 V (sample 7), which are less than the base metals. The Tafel outcomes of the specimens are shown in Table II. From the Tafel data, the sample 3 has higher corrosion current (I_{corr}) than the sample 6 in the absence of an inhibitor. Also, the welding process modified the samples towards the cathodic region when compared to the aluminium e.m.f. of –1.66 V. The recorded Tafel plots are presented in Fig. 5a–i. All plots show a slight difference in corrosion potential and corrosion current except the samples 2, 3 and 7. This result has revealed the rotating rpm impact on the corrosion resistance character. According to the electrochemical principle, when there is a rise in corrosion potential, it may be ascribed to either a decrease in the anodic reaction with the growth of a passive layer, or an increase in the cathodic reaction with an increase in dissolved oxygen; when there is a drop in corrosion potential, it can be attributed to the opposite of these two factors.[26,27] In addition, the Tafel plots are showing a positive side shift which is called anodic polarization. Anodic polarization causes higher corrosion initially and passive at last. But the corrosion potential is not significantly related to the corrosion rate. The corrosion current is directly related to the corrosion rate and converted to mm per year (mpy):

$$\text{Corr. rate (mpy)} = \\ = 0.13 I_{corr}\ (\mu\text{A cm}^{-2}) \times ((\text{eq. wt. of Al} = 9/(\text{density of Al} = 2.7)) \quad (1)$$

TABLE II. Potentiodynamic Tafel outcomes of the samples in the absence of an inhibitor; E_{corr} – corrosion potential; b_c – Tafel slope cathodic; b_a – Tafel slope anodic; I_{corr} – corrosion current density; Corr. rate – corrosion rate

Sample ID	E_{corr} / mV	b_c / mV dec^{-1}	b_a / mV dec^{-1}	I_{corr} / μA cm^{-2}	Corr. rate, mpy
6061	–1132	141.4	233.7	1.006	4.359
8011	–1110	207.3	158.5	1.010	4.377
2	–949	227.8	168.0	1.1	4.767
3	–1013	302.8	164.4	3.687	15.977
5	–1041	184.4	154.3	0.5541	2.401
6	–1008	196.6	191.3	0.5033	2.181
7	–1071	209.0	153.8	0.9134	3.958
9	–963	197.8	164.0	0.6642	2.878
10	–1044	193.0	157.0	0.5750	2.492

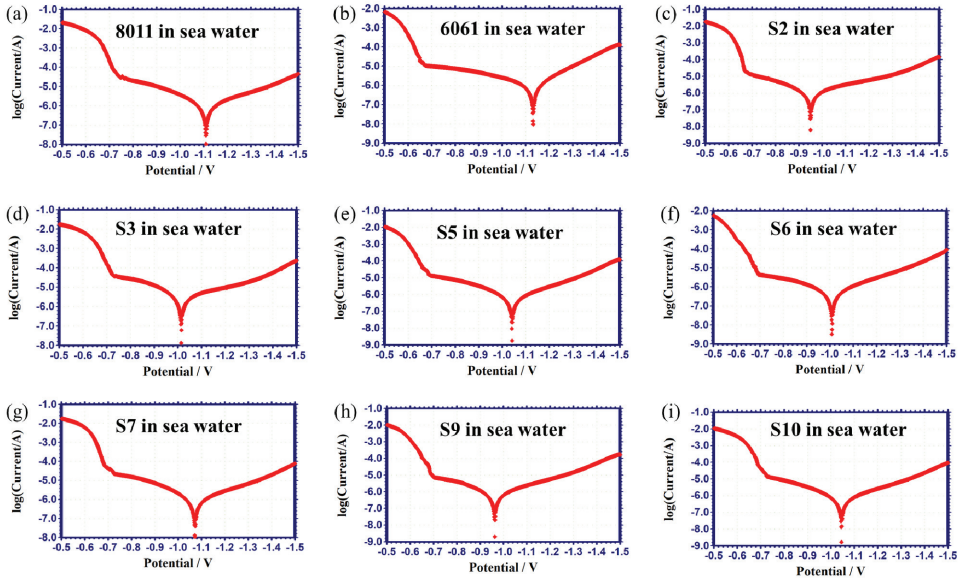

Fig. 5. Tafel plots of samples in sea water: a) base metal Al8011, b) base metal Al6061 and samples: c) 2, d) 3, e) 5, f) 6, g) 7, h) 9 and i) 10.

From Table II, this research finds a higher corrosion rate for sample 3 (15.977 mpy) and a lower one for sample 6 (2.181 mpy). Also, it has been found that the order of corrosion rate is sample 3 > sample 2 > sample 7 > sample 9 > sample 10 > sample 5 > sample 6. The last four samples have exposed the reduced corrosion rate when compared with the base metal rate. The samples at low rpm between 600 and 700 have shown good corrosion control. Similarly, higher rpm between 1000 and 1050 has exposed corrosion resistance when compared to the base metals. This work tried to enhance the corrosion resistance of the

samples using natural turmeric organic extract and $ZnSO_4$ salt to control the corrosion.[28–30]

Similarly, the potentiodynamic study conducted for the prepared test samples used curcumin as an organic inhibitor with zinc sulphate as a complexing agent for the electron transformation reaction. The results of the potentiodynamic study, along with the inhibitor mixture, are shown in Table III.[31–33] The changes in corrosion potentials are observed when compared to the cases with the absence of inhibitors. The potential is observed between –1.116 and –0.989 V. These values are somehow less than AA6061 potential and close to AA8011. From the corrosion current values, the corrosion rate was calculated in this work and it is shown in Table III.

TABLE III. Potentiodynamic Tafel outcomes of the samples in the presence of inhibitor; E_{corr} – corrosion potential; b_c – Tafel slope cathodic; b_a – Tafel slope anodic; I_{corr} – corrosion current density; Corr. rate – corrosion rate

Sample ID	E_{corr} / mV	b_c / mV dec^{-1}	b_a / mV dec^{-1}	I_{corr} / μA cm^{-2}	Corr. rate, mpy
6061	–1160	136.46	273.15	0.9971	4.321
8011	–1013	180.15	181.55	0.3820	1.655
2	–1095	158.03	382.26	1.831	7.934
3	–1116	258.26	196.93	7.652	33.159
5	–1006	127.94	213.17	0.1411	0.611
6	–1015	148.68	192.94	0.1543	0.669
7	–1115	229.36	188.22	4.950	21.450
9	–989	189.18	165.1	0.5509	2.387
10	–1011	157.98	202.51	0.1994	0.864

The calculated values show corrosion rates between 33.159 and 0.611 mpy. Based on the outcomes, the samples are arranged in the increasing order of their corrosion rate as sample 3 > sample 7 > sample 2> sample 9 > sample 10 > sample 6 > sample 5. Out of the seven samples, the samples 5, 6 and 10 have shown reduced corrosion rate when compared to all samples which include base metals represented in Fig. 6. Low rpm and high rpm samples show good control against corrosion and moderate speed affects the corrosion rate. The sample with a medium rotational speed and less penetration exhibits higher corrosion rates.

After the corrosion rate calculation in the presence of inhibition, linear polarization resistance (*LPR*) test was conducted in both the absence and the presence of inhibitors.[34–37] An *LPR* test, also known as a linear polarization resistance test, is a method for measuring the rate of corrosion, and it can provide an indicator of how resistant various materials are to corrosion in an aqueous environment.[38] Tests of *LPR* were carried out while the system was in a static state and also while it was moving back and forth. The corrosion potential and the corresponding current were measured in the potential between 10 and 20 mV. The resultant potential difference between the applied potential and the corrosion

potential *versus* the applied current, ($E_{app} - E_{corr}$) *vs.* I_{app} (positive anodic and negative cathodic) was used to plot the graph. The polarization resistance (*Rp*) was calculated using the slope value between the potential and the current density plot near E_{corr}. The relation between resistant potential and the current difference is:

$$Rp = \text{potential dif. } (\Delta E)/\text{current dif. } \Delta i \ (\Delta E \rightarrow 0) \quad (2)$$

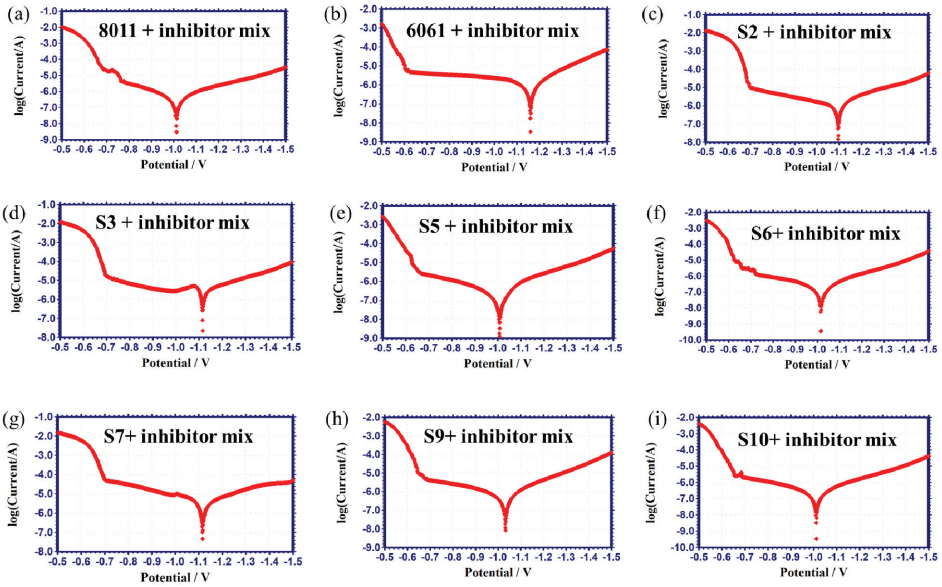

Fig. 6. Tafel plots of samples with inhibitor: a) base metal Al8011, b) base metal Al6061 and samples: c) 2, d) 3, e) 5, f) 6, g) 7, h) 9 and i) 10.

The outcomes exposed the inverse proportion of *LPR* with respect to the corrosion rate. When compared to the absence of inhibition, the corrosion rate is decreased in the presence of inhibition. The samples of *LPR* outcomes at both conditions are shown in Table IV. The graphical representation has shown the rotational speed impact on the corrosion current and lower than the base metal. The samples 5, 6 and 10 have shown higher corrosion resistance. The results have revealed that the rotational speed had an impact on the corrosion resistance. Lower rpm results in a big grain size and higher rpm shows small grains with high penetration being the reasons for the higher corrosion resistance. The successful optimization of BOBTFS welded samples shows the difference in the corrosion resistance in the presence and the absence of natural inhibitors. Organic curcumin binds with zinc sulphate and becomes a complex. Due to this nature, the molecule may be a good electron donor which donates an electron to the

welded samples in the salt solution and modifies the atmospheric salt solution. In addition to this Zn acts as an active anode when compared to aluminium.[39]

TABLE IV. Samples of *LPR* outcomes (Ω cm^2)

Sample ID	Condition	
	Absence of inhibitor	Presence of inhibitor
6061	38107	39682
8011	38683	102924
2	38222	26544
3	12563	6349
5	65934	246378
6	83759	236675
7	42178	9080
9	58686	69578
10	65461	193500

CONCLUSIONS

In this study, the effect of the bobbin tool welding process of aluminium on the corrosion behaviour of welded AA6061 aluminium with AA8011 alloy was investigated, and the following conclusions were drawn:

– In comparison with the base metal region, the welded area exhibited a more cathodic behaviour and a higher level of resistance to corrosion in the salt medium.

– The heat treatment technique boosted the corrosion potential of the source metal to more positive values, which is a desired outcome.

– The cathodic sites were provided by coarse metallic particles that were rich in aluminium and acted in relation to the matrix.

– Al 8011 had a greater resistance to corrosion in salt water than aluminium AA6061.

– Even in the presence of an inhibitor system, aluminium 8011 had a higher resistance to corrosion than aluminium 6061.

– In the presence of an inhibitor system, the corrosion resistance of the aluminium metals was improved.

– In the presence of an inhibitor system, the corrosion resistance of the following system decreased: sample 2, sample 3, sample 4 and the sample 7.

– In the presence of an Inhibitor system, the sample 5 system was the best one and the sample 6 was the next best.

– Also, this work observed optimized conditions such as lower rpm and higher rpm at a constant 40 mm/min.

– The inhibition of curcumin was enhanced by adding $ZnSO_4$ solution and achieved in the test aluminium samples.

– Keto-enol tautomerism and the hydroxyl group of the compounds could be the reasons for the improved corrosion resistance in BOBTFSW aluminium samples.

Acknowledgement. The authors are very much thankful to St.Joseph's College of Engineering.

И З В О Д

ПРОУЧАВАЊЕ ИНХИБИТОРНИХ ЕФЕКАТА ЕКСТРАКТА КУРКУМИНА НА РАЗЛИЧИТЕ АЛУМИНИЈУМСКЕ СПОЈЕВЕ

KAMATCHI PRAVINKUMAR, VADDI SESHAGIRI RAO и SATHISH RENGARAJAN

Department of Mechanical Engineering, St. Joseph's College of Engineering, OMR, Chennai-119, India

Алуминијумски заварени спојеви су све занимљивији за истраживаче због замене тешких челичних конструкција и смањења тежине компоненти које се користе у аутомобилском и поморском окружењу. У овој студији AA6061 и AA8011 су заварени коришћењем методе заваривања трењем и мешањем, помоћу алата са калемом, уз варирање параметара процеса са узорцима изложеним корозивном окружењу. Корозивна природа заварених легура у одсуству и присуству инхибитора (куркумин) је испитана електрохемијским методама и упоређена са сировим узорцима. Уочен је однос између 0,075 и 5,42 A cm^{-2}. Резултати показују да се контрола корозије побољшава спојем од легуре алуминијума AA6061 и AA8011 у присуству екстракта куркумина.

(Примљено 24. априла, ревидирано 1. јуна, прихваћено 8. октобра 2023)

REFERENCES

1. A. Heinz, A. Haszler, C. Keidel, S. Moldenhauer, R. Benedictus, W.S. Miller, *Mater. Sci. Eng., A* **280** (2000) 102 (https://doi.org/10.1016/s0921-5093(99)00674-7)
2. T. Dursun, C. Soutis, *Mater. Des.* **56** (2014) 862 (https://doi.org/10.1016/j.matdes.2013.12.002)
3. J. Hirsch, *Trans. Nonferrous Met. Soc. China* **24** (2014) 1995 (https://doi.org/10.1016/S1003-6326(14)63305-7)
4. C.H. Ng, S. N. M. Yahaya, A. A. A. Majid, *Acad. J. Sci. Res*. **5** (2017) 708 (https://academiapublishing.org/journals/ajsr/pdf/2017/Dec/Ng%20et%20al.pdf)
5. T. Trzepiecinski, *Metals* **10** (2020) 779 (https://doi.org/10.3390/met10060779)
6. D. Feron, *Corrosion Behaviour and Protection of Copper and Aluminium Alloys in Seawater,* Europ. Fed. Corros. Ser., 2007, pp. 145–155 (eBook ISBN: 9781845693084)
7. T. Watanabe, H. Takayama, A. Yanagisawa, *J. Mater. Process. Technol.* **178** (2006) 342 (https://doi.org/10.1016/j.jmatprotec.2006.04.117)
8. M. Khafri, *J. Mater. Sci.* **39** (2004) 6467 (https://doi.org/10.1023/B:JMSC.0000044884.25589.9b)
9. M. Esmaily, N. Mortazavi, W. Osikowicz, *Mater. Des.* **108** (2016) 114 (https://doi.org/10.1016/j.matdes.2016.06.089)
10. W. Y. Li, T. Fu, L. Hutsch, J. Hilgert, F. F. Wang, J. F. Dos Santos, N. Huber, *Mater. Des.* **64** (2014) 714 (https://doi.org/10.1016/j.matdes.2014.07.023)
11. K. Xhanari, M. Finsgar, *Int. J. Electrochem. Sci.* **12** (2017) 5845 (https://doi.org/10.20964/2017.07.71)

12. J.C. Swearengen, *Mater. Sci. Eng.* **10** (1972) 103 (https://doi.org/10.1016/0025-5416(72)90074-2)
13. J. Fayomi, A.P.I. Popoola, O.M. Popoola, O.S.I. Fayomi, *J. Alloys Compd*. **850** (2021) 1 (https://doi.org/10.1016/j.jallcom.2020.156679)
14. C. Shujin, Li. Hao, Lu. Sheng, Ni. Ruiyang, D. Jianghui, *Int. J. Adv. Manuf. Technol.* **86** (2016) 337 (https://doi.org/10.1007/s00170-015-8116-9)
15. D. Ji-Hong, G. Chong, L. Yao, H. Jain, J. Xiang-Dong, Z. Zhi-Xiong, *Int. J. Min. Met. Mater.* **24** (2017) 171 (https://doi.org/10.1007/s12613-017-1392-7)
16. R. Rosliza, W.B. Wan Nik, H.B. Senin, *Mater. Chem. Phys*. **107** (2008) 281 (https://doi.org/10.1016/j.matchemphys.2007.07.013)
17. M. K. Abbass, K. S. Hassan, A. S. Alwan, *Int. J. Manuf. Mater. Mech. Eng*. **3** (2015) 31 (https://doi.org/10.7763/IJMMM.2015.V3.161)
18. N. Sunitha, K.G. Manjunatha, S. Khan, M. Sravanthi, *SN Appl. Sci.* **1** (2019) 1024 (https://doi.org/10.1007/s42452-019-1063-6)
19. M. Mardalizadeh, M. Khandaei, M. Safarkhanian, *J. Adhes. Sci. Technol*. **35** (2020) 1 (https://doi.org/10.1080/01694243.2020.1792156)
20. M. K. Sued, D. Pons, J. Lavroff, E. H. Wong, *Mater. Des.* **54** (2014) 632 (https://doi.org/10.1016/j.matdes.2013.08.057)
21. M. M. Z. Ahmed, M. I. A. Habba, M. M. El-Sayed Seleman, K. Hajlaoui, S. Ataya, F. H. Latief, A. E. El-Nikhaily, *Materials* **14** (2021) 4585 (https://doi.org/10.3390/ma14164585)
22. W. Y. Li, T. Fu, L. Hutsch, J. Hilgert, F. F. Wang, J. F. Dos Santos, N. Huber, *Mater. Des.* **64** (2014) 714 (https://doi.org/10.1016/j.matdes.2014.07.023)
23. Y. Li, D. Sun, W. Gong, *Metals* **9** (2019) 894 (https://doi.org/10.3390/met9080894)
24. S. Sinhmar, D. K. Dwivedi, *Corros. Sci.* **133** (2018) 25 (https://doi.org/10.1016/j.corsci.2018.01.012)
25. F. Gharavi, K. A. Matori, R. Yunus, N. K. Othman, *Mater. Res.* **17** (2014) 672 (https://doi.org/10.1590/S1516-14392014005000053)
26. X. G. Zhang, *Corrosion and Electrochemistry of Zinc*, 1st ed., Springer, New York, 1996, pp. 125–156 (https://doi.org/10.1007/978-1-4757-9877-7_5)
27. S. B. Strbac, R. R. Adzic, in *Encyclopedia of Applied Electrochemistry*, G. Kreysa, K. Ota, R. F. Savinell, Eds., Springer, Berlin, 2014, p. 417 (https://doi.org/10.1007/978-1-4419-6996-5_485)
28. H. Elmsellem, M. H. Youssouf, A. Aouniti, T. Ben Hadda, A. Chetouani, B. Hammouti, *Russ. J. Appl. Chem*. **87** (2014) 744 (https://doi.org/10.1134/s1070427214060147)
29. L. Juhaiman, *Green Sustain. Chem.* **6** (2016) 57 (https://doi.org/10.4236/gsc.2016.62005)
30. E. A. Flores-Frias, V. Barba, R. Lopez-Sesenes, L. L. Landeros-Martinez, J. P. Flores-De Los Rios, M. Casales, J. G. Gonzalez-Rodriguez, *Int. J. Electrochem. Sci*. **14** (2019) 5026 (https://doi.org/10.20964/2019.06.53)
31. Y. Yan, *Metal. Biomed. Devices.* **1** (2010) 178 (https://doi.org/10.1533/9781845699246.2.178)
32. Y. Yan, A. Neville, and D. Dowson, *J. Phys., D* **39** (2006) 3200 (https://doi.org/10.1088/0022-3727/39/15/S10)
33. J. G. Speight, P. J. Subsea, *Deepwater Oil and Gas Science and Technology*, 1st ed., Gulf Professional, Oxford, 2012, p. 213 (https://doi.org/10.1016/B978-1-85617-558-6.00008-8)

34. F. Gharavi, K. Matori, R. Yunus, N. Othman, F. Fadaeifard, *J. Mater. Res. Technol.* **4** (2015) 314 (https://doi.org/10.1016/j.jmrt.2015.01.007)
35. R. Rosliza, W. B. Wan Nik, *Curr. Appl. Phys.* **10** (2010) 221 (https://doi.org/10.1016/j.cap.2009.05.027)
36. J. M. G. De Salazar, A. Urena, S. Manzanedo, M. I. Barrena, *Corr. Sci.* **41** (1998) 529 (https://doi.org/10.1016/s0010-938x(98)00135-8)
37. S. T. Selvamani, *J. Mater. Res. Technol.* **15** (2021) 315 (https://doi.org/10.1016/j.jmrt.2021.08.005)
38. K. Hornbostel, C. K. Larsen, M. R. Geiker, *Cement Concrete Composites* **39** (2013) 60 (https://doi.org/10.1016/j.cemconcomp.2013.03.019)
39. B. T. Ogunsemi, T. E. Abioye, T. I. Ogedengbe, H. Zuhailawati, *J. Mater. Res. Technol.* **11** (2021) 1061 (https://doi.org/10.1016/j.jmrt.2021.01.070).